



Cycle behaviour of hydrogen bromine redox flow battery cells with bromine complexing agents

Michael Küttinger^{a,b,*}, Ruben Brunetaud^a, Jakub K. Włodarczyk^c, Peter Fischer^a, Jens Tübke^{a,b}

^a Department of Applied Electrochemistry, Fraunhofer Institute for Chemical Technology ICT, Joseph-von-Fraunhofer-Straße 7, D-76327, Pfinztal, Germany

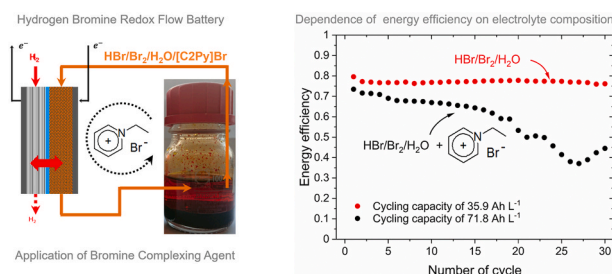
^b Institute for Mechanical Process Engineering and Mechanics, Karlsruhe Institute of Technology KIT, Straße am Forum 8, D-76131, Karlsruhe, Germany

^c Institute of Computational Physics (ICP), Zurich University of Applied Sciences (ZHAW), Wildbachstrasse 21, CH-8400, Winterthur, Switzerland

HIGHLIGHTS

- [C2Py]Br as bromine complexing agent in safe polysolutes for H₂/Br₂-RFB.
- Two-phase electrolyte: bromine-poor aqueous phase and bromine-rich fused salt.
- Bromine half cell performance limitation due to formation of [C2Py]-fused salt.
- Membrane performance limitation due to interaction with [C2Py]⁺ cations.
- Br₂ crossover intensifies both effects due to release of BCA from fused salt.

GRAPHICAL ABSTRACT



ARTICLE INFO

Keywords:

Stationary energy storage
Redox flow battery
Bromine
Safety
Bromine complexation
Cell performance

ABSTRACT

Bromine complexing agents (BCA) are used to improve the safety of aqueous bromine electrolytes versus bromine outgassing in bromine electrolytes. In this work, cycling performance of hydrogen-bromine redox flow battery cells with 1-ethylpyridin-1-ium bromide ([C2Py]Br) as BCA in a bromine electrolyte with a theoretical capacity of 179.6 A h L⁻¹ is investigated for the first time. The BCA leads to increased ohmic overvoltages. One cause of the ohmic drop can be attributed to [C2Py]⁺ cation interaction with the perfluorosulfonic acid (PFSA) membrane, which results in a drop of its conductivity. The BCA also interacts with bromine in the cell, by forming a non-aqueous fused salt second phase which exhibits a ten times lower conductivity compared to the aqueous electrolyte. A steep rise in cell voltage at the beginning of the charge curve followed by a regeneration of the cell voltage is attributed to this effect. Electrolyte crossover leads to an accumulation of [C2Py]⁺ in the electrolyte solution and intensifies both adverse processes. Under this condition only 30% of the theoretical electrolyte capacity of 179.6 A h L⁻¹ is available under long term cycle conditions. However, electrolyte capacity is high enough to compete with other flow battery technologies.

1. Introduction

One opportunity for stationary energy storage are hydrogen-bromine

redox flow batteries (H₂/Br₂-RFB) [1–5], which are currently on the cusp of commercialization [6,7]. H₂/Br₂-RFBs use a hydrogen gas diffusion electrode like in polymer electrolyte membrane fuel cells and a

* Corresponding author. Department of Applied Electrochemistry, Fraunhofer Institute for Chemical Technology ICT, Joseph-von-Fraunhofer-Straße 7, D-76327, Pfinztal, Germany.

E-mail address: michael.kuettinger@gmx.de (M. Küttinger).

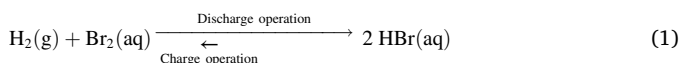
<https://doi.org/10.1016/j.jpowsour.2021.229820>

Received 18 December 2020; Received in revised form 11 March 2021; Accepted 18 March 2021

Available online 1 April 2021

0378-7753/© 2021 The Authors. Published by Elsevier B.V. This is an open access article under the CC BY license (<http://creativecommons.org/licenses/by/4.0/>).

bromine/bromide half cell, which is operated with liquid electrolytes. Electrolytes are composed of hydrobromic acid (HBr), bromine (Br_2) and water and are pumped through the positive H_2/Br_2 -RFB half cell. The principle of a H_2/Br_2 -RFB is shown in Fig. 1/a. During charge, bromide (Br^-) is converted to Br_2 by oxidation in the positive half cell. In the negative half cell protons (H^+) are reduced to hydrogen (H_2) [3,4]. Discharging of the battery takes place in the same conversion unit, while the reactions proceed in opposite direction [3,4] according to equation Eq. (1) [4,11]. The open cell voltage at standard conditions is 1.09 V [8–10].



High possible molar substance concentrations in the electrolytes (e.g. 7.7 M HBr) lead to large useable capacities of 179.6 A h L^{-1} [12]. Also high power densities can be reached [3,13]. Both are raised due to fast reaction kinetics in both half cells and high concentrations of HBr and Br_2 [3,13]. Instead, other redox flow battery (RFB) types like vanadium-RFB are limited in their volumetric electrolyte energy density of around $26.8 \text{ Wh L}^{-1}/21.4 \text{ A h L}^{-1}$ [6] and in zinc bromine RFB (Zn/Br_2 -RFB) the zinc deposition on the electrode surface limits the storage capacity [14,15].

The high solubility of unpolar Br_2 in HBr solutions [16,17] is reached

due to the formation of so-called polybromides Br_{2n+1} like tri-, penta- and heptabromides according ref. [5,8,12,18–21]. Those are bound by addition bonds to the bromine ion [22]. Nevertheless, bromine remains highly volatile due to its high vapour pressure [23–25] and is toxic by skin contact and inhalation [15,26]. In order to achieve safe and high energy density battery electrolytes, bromine complexing agents (BCA) are applied to reduce vapour pressure of bromine in aqueous solutions [24]. There, mainly BCAs from the group of quaternary ammonium salts are used as complexing agents [27–32]. Common substances, which are mainly applied in Zn/Br_2 -RFB since the 1970s are 1-ethyl-1-methylpyrrolidin-1-ium bromide [MEP]Br and 1-ethyl-1-methylmorpholin-1-ium bromide [MEM]Br [14,26–28,32–42]. Next to [MEP]Br and [MEM]Br there is a wide range of possible BCAs based on quaternary ammonia moiety, which are made from N-heterocycles [14,26,28,31,32,37,38,41,42]. 1-ethylpyridin-1-ium bromide [C2Py]Br (Fig. 1/b) is a cost effective BCA and is suggested by other authors due to moderate sequestration and lower polarization effects in the cell compared to other BCAs [14,41], but only investigated for Zn/Br_2 -RFB application with a focus on zinc deposition. The functionality of these BCAs is based on the obtained solubility of the BCA-bromide salt while precipitation of BCA-polybromide salts occurs according to Eq. (2) [22,27,31], resulting in the formation of an additional phase as shown in Fig. 1/a for the example of [C2Py]Br. This phase does not form a solid, but a second

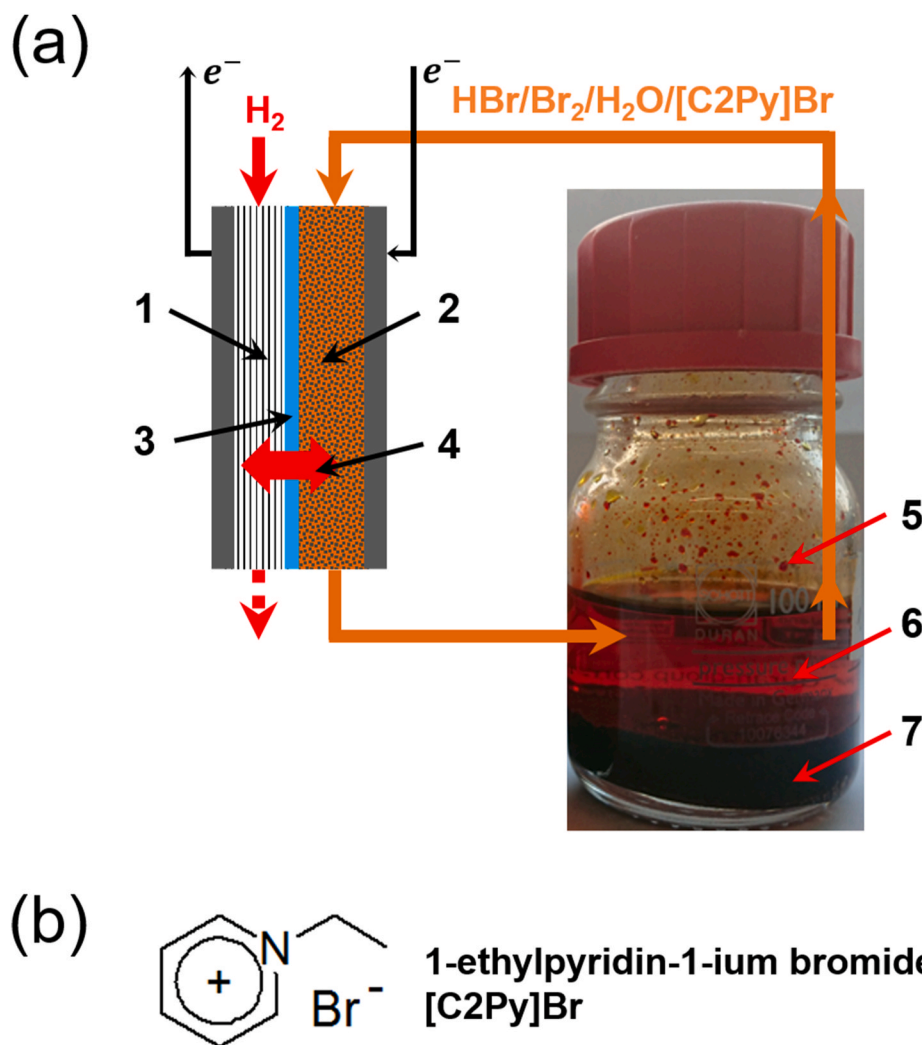


Fig. 1. (a) Schematic drawing of assembly and operation of a H_2/Br_2 -RFB single cell ((1) hydrogen gas diffusion half cell, (2) positive bromine half cell, (3) PFSA membrane, (4) proton exchange through membrane) with inserted photograph showing the phase compositions of a bromine electrolyte with BCA containing (5) Br_2 in gas phase, (6) aqueous electrolyte phase and (7) fused salt in a glass tank and (b) structural formula of the applied BCA 1-ethylpyridin-1-ium bromide [C2Py]Br.

liquid phase [14,41] at room temperature, very similar to a deep eutectic phase, and is called fused salt. It deposits below the aqueous solution due to its high density (Fig. 1/a) [31]. During charge and discharge experiments, polybromides, $[C2Py]^+$ cations and bromide are distributed across two different phases based on Eq. (2):



The application of BCAs in acidic solution for H_2/Br_2 -RFB has not been investigated in detail. No comprehensive study on cycling tests with $[C2Py]Br$ or further BCAs in electrolytes for H_2/Br_2 -RFB has been presented in the literature so far, with the aim of achieving a durable battery cycleability and considering an electrolyte with a large theoretical capacity of 179.6 A h L^{-1} and a large theoretical energy density of 195.8 Wh L^{-1} . A dependence of the processes in cell based on Eq. (2) and on the state of charge (SoC) considering the associated electrolyte compositions has not been investigated in a cell test so far.

In this study we investigate the influence of the bromine complexing agent $[C2Py]Br$ on the cell performance of a H_2/Br_2 -RFB single cell. High energy density electrolyte with a theoretical capacity of 179.6 A h L^{-1} is chosen. Cycling experiments along the capacity range are determined for different electrolytes. Visible phenomena caused of $[C2Py]Br$ and their influence on the cell performance are determined in analytical methods online and in ex situ investigations on electrolyte composition. This study focuses especially on the comparison between $[C2Py]^+(aq)$ concentrations and cell performance, and effects on further parameters like electrolyte conductivity, bromine concentrations and cell resistances. The work provides a detailed investigation on challenges in the application of quaternary ammonium compounds as BCAs in the bromine half cell of a H_2/Br_2 -RFB. In Section 2 experimental methods are described for this purpose. Results are presented and discussed in Section 3.

2. Experimental and methods

A detailed version of the chapter “Experimental and methods” is available in the Electronic Supplementary Information (ESI). There, individual methods are described in detail in order to allow for experiments to be reproduced. Furthermore, substances and materials used, their suppliers, purity, measurement setup and NMR characterization of the synthesized $[C2Py]Br$ can also be found in the ESI.

2.1. Electrolyte preparation

Bromine electrolytes base on HBr 48 wt% and Br_2 in aqueous solution. The targeted capacity is specified by the composition at different state of charge (SoC): SoC 0% with 7.7 M HBr and SoC 100% with 1 M HBr and 3.35 M Br_2 . The definition of the SoC range is based on an work in earlier literature [12] concerning BCA-free HBr/ Br_2 / H_2O electrolytes. The concentration of the $[C2Py]Br$ is 1.11 M for all BCA-containing electrolyte samples. The choice of BCA concentration depends on the molar ratio of Br_2 to BCA at certain SoCs. A ratio of 3:1 between Br_2 and BCA is received at SoC 100%, representing theoretically one molecule heptabromide Br_7^- for each BCA molecule in solution. At SoC 33% respectively a ratio of 1:1 between Br_2 and BCA is received, expecting all Br_2 to be available as tribromide Br_3^- . $[C2Py]Br$ is prepared from pyridine and bromoethane by alkylation [43,44] according to Dzyuba et al. [45] and dried in a vacuum chamber. 1H NMR and ^{13}C NMR (attached in ESI) are recorded for $[C2Py]Br$ and confirmed by existing literature [44]. $[C2Py]Br$ is solved in water and HBr 48 wt% and after Br_2 is added. Equilibrium of the components across the two phases is reached by mixing electrolyte samples each day once for one week. For ex situ investigation of electrolyte properties 30 mL samples of electrolytes at SoC 0, 33, 60, 66, 70, 80, 90 and 100% are mixed. For all cycling tests 90 mL of electrolyte at SoC 100% are prepared. Choice of SoC for the investigated samples is based on the investigated SoC range in cell tests

(Section 2.6). All measurements on the electrolytes are carried out at a temperature of $\vartheta = 23 \text{ }^\circ\text{C} \pm 1 \text{ }^\circ\text{C}$.

2.2. Electrolyte conductivities

Electrolytic conductivities of aqueous electrolyte solutions and fused salts for SoC 0, 33, 60, 66, 70, 80, 90 and 100% are determined with a conductivity cell. Ohmic electrolyte resistances are measured by electrochemical impedance spectroscopy at $\vartheta = 23 \text{ }^\circ\text{C} \pm 1 \text{ }^\circ\text{C}$ with a perturbation of $\hat{u} = \pm 10 \text{ mV}$ between the frequencies of 1 MHz and 1 Hz. Ohmic resistances of the electrolytes are determined and conductivities calculated. Determination of cell constant and further description are given in ESI.

2.3. Concentration of Br_2 in aqueous solution

Concentrations of Br_2 in the equilibrated aqueous phase of $[C2Py]Br$ electrolytes at SoC 0, 33, 60, 66, 70, 80, 90 and 100% are investigated by linear chronoamperometry at a rotating disk electrode. At a rotation speed (ω) of $\omega = 1000 \text{ rpm}$ on vitreous carbon electrode, linear sweep excitations between 0.8 V and -0.5 V vs. $Ag/AgCl/KCl(sat.)$ reference electrode (RE) and a scan rate of -40 mV s^{-1} are performed. Constant reduction reaction currents result for potentials $< -0.1 \text{ V}$ vs. RE, which are independent of the applied potential. According to Levich [46–49], these reduction currents are directly proportional to the concentration $c(Br_2)$ of the bulk solution. Concentrations $c(Br_2(aq))$ (SoC) are calculated from the limiting currents $I_{diff,lim}$ (mA) by Eq. (3), based on a calibration measurement with known Br_2 concentrations described in the ESI.

$$c(Br_2(aq)) = m \cdot I_{diff,lim} \quad (3)$$

The calibration constant m is $0.00342466 \text{ mol L}^{-1} \text{ mA}^{-1}$, while for Br_2 concentrations the unit mol L^{-1} is applied. For different electrolytes depending on the chosen SoC, different Br_2 concentrations are measured due to individual limiting currents.

2.4. $[C2Py]Br$ concentration in the aqueous phase

Concentrations of $[C2Py]Br$ in equilibrated aqueous solutions at SoC 0, 33, 60, 66, 70, 80, 90 and 100% and of further samples of aqueous phase in the bulk solutions during a cell test are detected with Raman spectroscopy at a Raman shift ($\tilde{\nu}$) of $\tilde{\nu} = 1030 \text{ cm}^{-1}$. At $\tilde{\nu} = 1030 \text{ cm}^{-1}$ the excitation of the aromatic structure of the pyridine is given [50–52]. Calibration is done with 1.11 M $[C2Py]Br$ in 7.7 M HBr solution. $[C2Py]^+(aq)$ concentrations are calculated by comparing peak areas at $\tilde{\nu} = 1030 \text{ cm}^{-1}$ of the measured solution with the 1.11 M $[C2Py]Br$ solution (ESI).

2.5. Test cell setup

Cell tests are performed at $\vartheta = 23 \text{ }^\circ\text{C} \pm 1 \text{ }^\circ\text{C}$ in a self-developed H_2/Br_2 -RFB single cell with a geometric membrane area of 40 cm^2 . A scheme of the setup is shown in the ESI (Figure S-1). The positive half cell contains a graphite felt electrode embedded in a flow frame. Electrolyte is stored in a capped glass tank. Aqueous bromine/bromide electrolyte is pumped through the felt electrode with a constant flow rate of 30 mL min^{-1} . The second fused salt phase stays in the tank and is not circulated. The current collectors' material is Glassy Carbon. Used membrane electrolyte assemblies (MEA) are Nafion®117 membranes, based on PFSA membrane technology, including a single side catalyst coating of 3 mg Pt cm^{-2} on carbon. The catalyst is used for the hydrogen reactions in the negative half cell. A graphite plate, with self-milled meander structure and gas diffusion layer (GDL) for the gas side supply is used as current collector in the negative hydrogen half cell. The negative hydrogen half cell is operated in a flow through mode but non-recyclable with a stoichiometric factor (λ) of $\lambda = 6.57$ and fed with dry H_2 of 100 mL min^{-1} during cycling (Fig. 1/a). The parameters

determined during the experiments are: Cell voltage $E_{\text{Cell } i \neq 0}$ under load, redox potential $\phi(\text{Br}_2/\text{Br}^-)_{\text{redox}}$ versus the normal hydrogen electrode (NHE) and half cell potentials of the positive bromine half cell $\phi(\text{Br}_2/\text{Br}^-)_{i \neq 0}$ vs. NHE and the negative hydrogen half cell $\phi(\text{H}^+/\text{H}_2)_{i \neq 0}$ vs. NHE. A so-called “residual voltage”, ΔE_{RES} is calculated from these values according to Eq. (4):

$$\Delta E_{\text{RES}} = E_{\text{Cell } i \neq 0} - (\phi(\text{Br}_2/\text{Br}^-)_{i \neq 0} - \phi(\text{H}^+/\text{H}_2)_{i \neq 0}) \quad [\Delta E_{\text{RES}}] = \text{V} \quad (4)$$

It essentially reproduces the overvoltages between the positive and the negative half cell and represents the sum of electrolyte and membrane resistances. Qualitatively noticeable occurrences of cell voltage behaviour are determined from the galvanostatic cycle test. Investigation focuses on the bromine half cell. The measurement setup is shown in detail in the ESI.

2.6. Cycling tests in H_2/Br_2 -RFB single cell

Galvanostatic cycling tests are performed at a current density of $i = \pm 50 \text{ mA cm}^{-2}$ between the voltage thresholds of +1.55 V and +0.20 V. The depth of discharge is determined by limiting the converted electrical charge during the experiment, as shown in Table 1. This results in maximum charge and discharge times for all cycle tests (Table 1). Two types of cell tests are carried out: For qualitative performance investigation (1) one test is performed starting in discharge operation mode from SoC 100% to 90% and back to 100%. After repeating this experiment for three times, the same procedure is applied to a depth of discharge to SoC 80%, SoC 70% and SoC 60% for three times each. In addition, for cycling durability (2), three tests starting from SoC 100% to SoC 80, 70 and 60% are investigated for 30 cycles each. The lower SoC threshold is defined as SoC 80, 70 and 60%. In this cell test also the mass loss of the bromine electrolyte is determined in parallel to the cycling test. The glass tank is placed on a balance and mass changes are recorded digitally over the time.

Cell tests are evaluated qualitatively by evaluating of the progression of voltages and potentials and quantitatively regarding average charge/discharge voltages ($\overline{E_{\text{C,N}}}$, $\overline{E_{\text{D,N}}}$, respectively) and charge/discharge capacities ($\Delta Q_{\text{C,N}}$, $\Delta Q_{\text{D,N}}$, respectively) quantitatively for each cycle N from cell voltage $E_{\text{Cell } i \neq 0}$ and current I along the cycling times [53]. Voltage efficiencies (VE), coulombic efficiencies (CE) and energy efficiencies (EE) are calculated following [54]. Between charge and discharge experiments ohmic cell resistances are measured by help of galvanostatic electrochemical impedance spectroscopy (EIS) with a perturbation of $\hat{i} = \pm 5 \text{ mA cm}^{-2}$ at open circuit voltage in the frequency range between 1 MHz and 1 Hz (ESI).

2.7. FT-IR investigation of membrane

Nafion®117 membranes, which are soaked in aqueous electrolyte solutions ex situ at SoC 0, 33, 60, 70, 80, 90 and 100%, are investigated by Fourier Transform Infrared Spectroscopy (FT-IR spectroscopy). Results are compared with the FT-IR spectra of the same membrane type in BCA-free $\text{HBr}/\text{Br}_2/\text{H}_2\text{O}$ samples at same SoCs. Details are explained in the ESI.

Table 1

SoC range of cycling tests starting from electrolytes having SoC 100%, represented as a function of the SoC for the maximum discharge point: converted charges and charge/discharge duration.

SoC range for cycling	Converted electrical charge $Q/\text{Ah L}^{-1}$	Charge, discharge time for ($i = \pm 50 \text{ mA cm}^{-2}$ and $V = 90 \text{ mL}/\text{h}$)
SoC 100-80%	35.91	1.616
SoC 100-70%	53.78	2.424
SoC 100-60%	71.83	3.232

3. Results and discussion

3.1. Fundamental properties of the electrolyte

Concentrations of $\text{Br}_2(\text{aq})$ and $[\text{C2Py}]^+(\text{aq})$ in the equilibrated aqueous phase vary over the SoC range of the electrolyte and are quite different from those in BCA-free electrolytes. Preliminary tests already showed a dependence of the cell performance on the choice of electrolyte: The difficulty in operating a H_2/Br_2 -RFB single cell with a BCA containing electrolyte starts with the first charging of the electrolyte. The electrolyte containing 1.11 M $[\text{C2Py}]\text{Br}$ cannot be cycled from chosen SoC 0%. Due to an increasing ohmic cell resistance the voltage thresholds are reached within some minutes of charge, when $[\text{C2Py}]\text{Br}$ is dissolved in the electrolyte. Similar behaviour has been described by Küttinger et al. [55] during application of $[\text{MEP}]\text{Br}$. Since this phenomenon only occurs when applying BCAs in solution, while charging of BCA-free electrolyte is possible [3,5,12], a strong influence of the $[\text{MEP}]^+$ and $[\text{C2Py}]^+$ cations is presumed.

To address the problem during charging, first the composition of the electrolyte at selected SoCs is investigated in detail ex situ. The concentrations of $\text{Br}_2(\text{aq})$, $[\text{C2Py}]^+(\text{aq})$ and the ionic conductivity of the aqueous electrolyte solution are shown in Table 2. While the concentration of total $\text{Br}_2(\text{aq})$ in BCA-free $\text{HBr}/\text{Br}_2/\text{H}_2\text{O}$ solution increases linearly with SoC and reaches values up to 3.35 M Br_2 , the concentration of $\text{Br}_2(\text{aq})$ is reduced when using $[\text{C2Py}]\text{Br}$ as BCA in aqueous electrolyte solutions. Therefore, lower quantities of Br_2 are pumped into the positive half cell for discharge operation. Simultaneously, the concentration of $[\text{C2Py}]^+(\text{aq})$ decreases, since these ions are transferred in the presence of polybromides into the fused salt according to Eq. (2). For SoC $\geq 70\%$, no $[\text{C2Py}]^+(\text{aq})$ is detected in the aqueous phase for electrolyte solutions in equilibrium. All $[\text{C2Py}]^+$ cations are transferred into the fused salt. Conductivities of the aqueous electrolyte (Table 2) increase between SoC 0 and 66%. The conductivity κ is high with $\kappa > 350 \text{ mS cm}^{-1}$ and therefore suitable for use in redox flow batteries. For SoC $\geq 66\%$ it decreases strongly due to decreasing proton concentration, shown in Ref. [12]. Protons are consumed by the cell reaction according to Eq. (1) during the charge process. The corresponding fused salt conductivity (Table 2) is with $51.6 \leq \kappa \leq 93.6 \text{ mS cm}^{-1}$ much lower compared to the conductivity of the aqueous phase. The result of $\text{Br}_2(\text{aq})$ and $[\text{C2Py}]^+(\text{aq})$ concentration as well as conductivities of both phases are introduced here to validate results of the cell tests within the following chapters.

3.2. Stepwise cycling of the H_2/Br_2 -RFB single cell

As a charge operation starting at SoC 0% is not possible (Section 3.1) an alternative approach to investigate cell cycling performance is applied: The cell is cycled within SoC steps, starting with galvanostatic discharge operation from SoC 100%, while step length is increased (SoC 100-90%, SoC 100-80%, SoC 100-70%, SoC 100-60%). From Section 3.1 it is known that the electrolyte is free of BCA at SoC 100%. Between each of these subsequent steps three galvanostatic cycles with constant charge/discharge times are operated with a current density of $\pm 50 \text{ mA cm}^{-2}$. The results are depicted in Fig. 2.

In general, cycling of the cell with this electrolyte between SoC 100-90% and SoC 100-80% is possible without difficulties, while anomalies in the cell voltage already occur in the cycling range SoC 100-70%. Cycling below SoC 70% is not possible with this electrolyte, whereby the $[\text{BCA}]^+$ cations in the positive half cell are considered to be responsible for this limitation:

In Fig. 2/a cell voltage (black) of the cycling test and the half cell potential of the positive bromine half cell (red) over the time are plotted and change over time. The half cell potential of the negative hydrogen half cell (blue) remains approximately constant for all cycles in comparison to the cell voltage and is therefore not influenced by the SoC or further effects during cycling. Small potential changes of this half cell

Table 2

Electrolyte properties of investigated electrolyte mixtures at specific SoCs for pure HBr/Br₂/H₂O electrolytes and electrolytes with [C2Py]Br as an additive: The concentration of Br₂ in the aqueous phase of a BCA-free HBr/Br₂/H₂O electrolyte with linear rise over the SoC range is compared to the concentration of Br₂ in the aqueous phase of the same electrolytes containing [C2Py]Br. For the electrolyte containing [C2Py]Br, the concentration of [C2Py]⁺ cations is investigated to show the sequestration process according to Eq. (2) and electrolyte conductivities of the aqueous phase (large) and the fused salt phase (low) are compared for this electrolyte for validation of results in the following cell tests.

State of Charge SoC/%	BCA-free HBr/Br ₂ /H ₂ O	[C2Py]Br electrolyte			Fused salt (fs)
	Aqueous (aq)	Aqueous (aq)		Conductivity (fs) at 23 °C ± 1 °C/ mS cm ⁻¹ [b]	
	Concentration of Br ₂ (aq)/M [a]	Concentration of Br ₂ (aq)/M [b]	Concentration of [C2Py] ⁺ (aq)/M [b]	Conductivity (aq) at 23 °C ± 1 °C/mS cm ⁻¹ [b]	
0	0	0	1.110	471.3	-
33	1.12	0.117	0.307	652.8	51.6
60	2.01	0.203	0.052	710.2	76.9
66	2.23	0.208	0.023	694.0	79.2
70	2.34	0.222	0 ^[c]	686.4	82.8
80	2.68	0.264	0 ^[c]	619.8	86.9
90	3.11 ^[d]	0.259	0 ^[c]	514.1	91.8
100	3.35 ^[d]	0.237	0 ^[c]	363.4	93.9

[a] calculated, [b] measured, [c] values below detection limit and [d] total concentration of Br₂ in sample, while for SoC 90% and SoC 100% in pure HBr/Br₂/H₂O a separate phase of pure Br₂ is formed (ref. [12]).

can be caused by mixed potentials on the hydrogen half cell due to crossover of bromine or loading of bromide onto the platinum catalyst or by an unstable reference electrode (setup explained in ESI) [56–58].

During the first six cycles (Fig. 2) there are no particular irregularities in the voltage and potential characteristics from cycling of BCA-free electrolytes (ref. [3,5,12]) and cell cycling between SoC 100-90% and SoC 100-80% is possible: The trend of the potential of the positive bromine half cell basically follows the trend of the cell voltage. Differences between cell voltage and potential of the positive half cell are nearly constant and result from the ohmic resistance of the cell at the constant current of ± 50 mA cm⁻². The potential change of the positive half cell depends primarily on the change of redox potential of the electrolyte, resulting in a parallel or almost identical curve between red and orange curves in Fig. 2/a. The difference between the positive half cell potential and the redox potential describes the overvoltage of the Br₂/Br⁻ reaction, which is negligible in this work due to fast reaction kinetics of the Br₂/Br⁻ couple. For discharge and charge operation during the first 6 cycles no mass transport limitation in the positive half cell is observed, as neither half cell potentials nor cell voltage show a strong increase or decrease at the end of the charge or discharge operation.

From the 7th cycle onwards (SoC 100-70%) performance of the cell becomes lower. Cell voltage decreases further during discharge (Fig. 2/a – depicted by “B”). At the same time, an increasing peak is observed at the beginning of each charge process (Fig. 2/a – depicted by “A”). The two half cell potentials do not follow this trend of the cell voltage. The half cell potential of the positive half-cell continues to follow the trend of the redox potential. The half cell potential of the hydrogen-electrode remains approximately constant. Both half cell observations exclude that the rise in cell overvoltage is based on slower reaction kinetics. Also mass transport limitation in front of the electrode can be excluded. In parallel, it is observed from the 9th cycle that during the charge process after cell voltage reaches the peak point “A”, with a time delay of around 0.5 h, individual red-brown drops of fused salt leave the positive half cell. [C2Py]⁺ cations of the aqueous phase are thought to cause fused salt formation (“A”) in the cell and lead during discharge (“B”) to higher cell resistance.

In the 10th cycle (for SoC 100-60%) the complete discharge process is still possible, but during charging the upper voltage limit of 1.55 V is reached, whereby the charging process is interrupted and another discharge process follows. From the 11th cycle onwards, charging and discharging are no longer possible as the upper and lower voltage thresholds are reached. The influence of [C2Py]⁺ cations described above in the anomalies “A” and “B” seems to be intensified in this region.

From the 7th cycle on discharge and charge tests are limited by

increasing overvoltages in the cell. As limitations of charge transfer resistance or the thermodynamic change of the cell voltage (redox potential Br₂/Br⁻), as well as mass transport limitation in front of the electrodes can be excluded, possible overvoltages must be due to the ohmic resistances, attributed to the electrolyte resistance and the membrane resistance. This is confirmed from the residual voltage ΔE_{RES}, which primarily indicates the anomaly of the cell voltage and approximately represents the sum of electrolyte and membrane overvoltages. Both phenomena “A” and “B” are discussed further in Section 3.3 and 3.4.

A further discharge to SoC ≤70% is not possible, leading to a maximum useable electrolyte capacity of around 53.9 A h L⁻¹ which constitutes only 30% of the targeted capacity of 179.56 A h L⁻¹. The possible operating range for the cell is limited to the SoC range between SoC 100% and 70%, while from lower SoCs, the cell cannot be charged again.

During the experiment, the ohmic cell resistance (Fig. 2/b) increases with increasing cycle numbers and discharge depth, starting from 0.98 Ohm cm², with slowly rising resistance values for the first six cycles measured before and after discharge process (SoC 100-90% and SoC 100-80%). From the 7th cycle on (SoC 100-70%) the ohmic cell resistances after discharge are increased compared to the values before discharge. From the 10th cycle on the ohmic resistances increase strongly. Since the voltage peak during charging (Fig. 2/a – depicted by “A”) occurs reversibly during the charging process, a rise of cell resistance can be suggested by interaction of [C2Py]⁺(aq) in the aqueous solution with the membrane.

In order to investigate both phenomena “A” and “B” in cell voltages in detail, both, charge and discharge processes, are considered separately by examination of electrolyte samples and analyzation of membrane samples in sections 3.3 and 3.4.

3.3. Investigation of the anomaly in voltage behaviour during the charge process

In order to study the phenomena in the positive half cell during the charge process marked with “A” in Fig. 2/a, a further cell test between SoC 100-60% is performed (Fig. 3/a) within the enlarged voltage threshold to 3.0 V, and showing again a strong voltage peak during charge operation. For the charge operation starting from SoC 60% at different times (Fig. 3/a), samples of the aqueous bulk solution in the electrolyte glass tank are collected and the concentration of [C2Py]⁺(aq) is examined by Raman spectroscopy. Raman spectra of [C2Py]⁺(aq) with a strong, single peak at $\tilde{\nu} = 1030.2 \text{ cm}^{-1}$ are obtained (Fig. 3/b). The concentration of [C2Py]⁺(aq) in aqueous phase decreases from 168

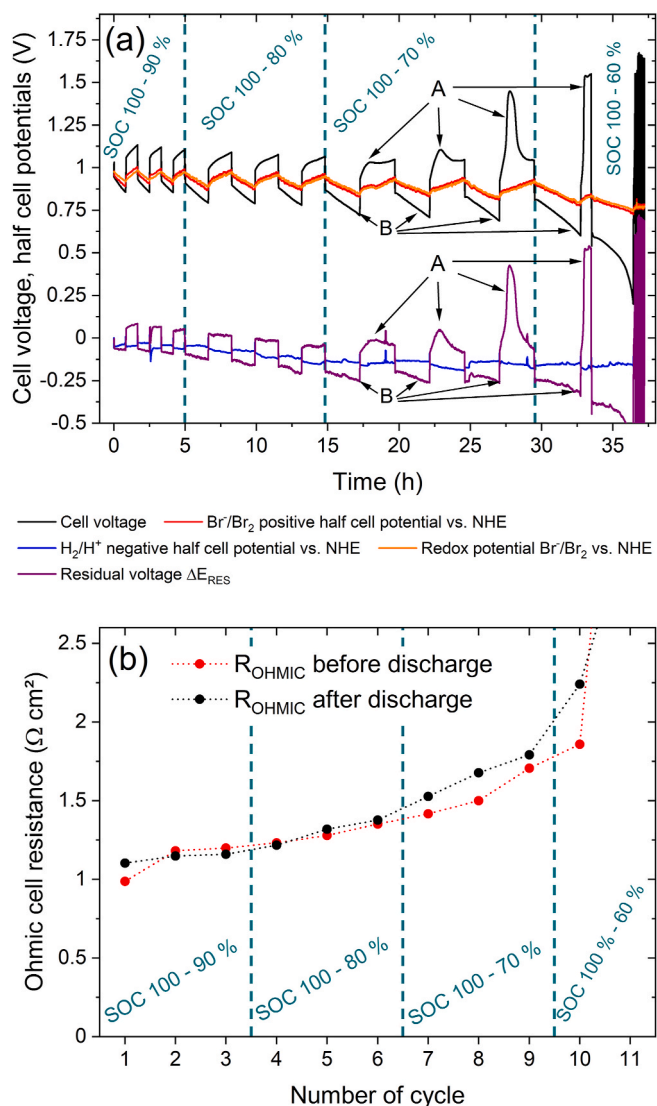


Fig. 2. Cycle tests at $\pm 50 \text{ mA cm}^{-2}$ with increasing discharge depth between SoC 100-90%, as well as SoC 100-80%, SoC 100-70% and SoC 100-60% by three cycles per SoC range: (a) cell voltage (black), potential of the positive bromine half cell vs. NHE (red), potential of the negative hydrogen half cell vs. NHE (blue), redox potential of the electrolyte at Glassy Carbon vs. NHE (orange) and residual voltage ΔE_{RES} (purple) as a function of time, and (b) associated ohmic cell resistances before and after discharge operation as a function of the number of cycles. In (a) the letters “A” and “B” show anomalies for the cell voltage related to the application of the BCA and are evaluated further in the following sections. (For interpretation of the references to colour in this figure legend, the reader is referred to the Web version of this article.)

mM at the beginning of the charge experiment and $[\text{C2Py}]^+(\text{aq})$ is no longer detectable after 105 min as shown in Fig. 3/c. These concentrations are measured online during charge. For comparison, the $[\text{C2Py}]^+(\text{aq})$ concentrations from Table 2 of electrolyte samples with their phases at equilibrium are shown in Fig. 3/c. As during cell operation at each time a specific SoC of the electrolyte is present, it is possible to compare concentrations of $[\text{C2Py}]^+(\text{aq})$ at equilibrium and during operation in the cell. It is obtained that $[\text{C2Py}]^+(\text{aq})$ concentrations of ex situ investigated samples at equilibrium from Table 2 are much lower than during the real discharge experiment. In addition, after reaching the voltage peak in Fig. 3/a again red-brown drops of fused salt flow through the outlet of the positive half cell back to the glass tank.

According to this results a formation of fused salt in the positive half cell is indicated during the charge and leading to high cell overvoltages.

This is based on three phenomena connected to each other: (i) At the beginning of the charging process the cell voltage rises sharply in the form of an ohmic overvoltage and after a certain time returns to expected values. At the same time (ii) the Raman measurements indicate, that $[\text{C2Py}]^+(\text{aq})$ cations are present in the aqueous electrolyte solution at the beginning of the charge process and their concentration decreases over time. Finally, (iii) with a certain time delay, viscous single droplets of fused salt flowing from the cell outlet into the tank are observed.

Therefore, the voltage peak during the charging process can be assigned to the formation and accumulation of fused salt $[\text{C2Py}]_{\text{Br}_{2n+1}}$ in the positive half cell and only occurs during charge operation (Eq. (2)). A prerequisite to form fused salt is the presence of dissolved $[\text{C2Py}]^+(\text{aq})$ cations in the aqueous phase and the formation of bromine in the positive half cell. During the preceding discharge process $[\text{C2Py}]^+$ cations are released from the fused salt phase into the aqueous electrolyte phase and are available in tenth-molar scale, as it is shown in (Fig. 3/b and c) at $t_1 = 0 \text{ min}$ with $c([\text{C2Py}]^+) = 168 \text{ mM}$. Even for electrolytes at equilibrium between the phases, dissolved $[\text{C2Py}]^+(\text{aq})$ cations in the aqueous phase for SoC < 70% are present, as shown in Table 2. In general during discharge process higher amounts of $[\text{C2Py}]^+(\text{aq})$ cations are released from the fused salt phase into the aqueous phase, compared to $[\text{C2Py}]^+(\text{aq})$ concentrations in equilibrium (Fig. 3/b).

During the charge process, bromide is oxidized at the electrode surface of the positive half cell and released into the aqueous electrolyte in the form of polybromides. If, however, $[\text{C2Py}]^+(\text{aq})$ cations are present, the resulting hardly soluble $[\text{C2Py}]$ -polybromide salts, form the liquid fused salt, and clog the porous felt. Electrolytic conductivities of the fused salt phase are examined, shown and compared with the conductivities of the aqueous electrolyte solutions in Table 2. Conductivities of the fused salt of $[\text{C2Py}]_{\text{Br}_{2n+1}}$ over the SoC range between 33% and 100% give values between 51.6 and 93.9 mS cm^{-1} , while the aqueous solution reaches conductivities from 363.4 mS cm^{-1} to 694.0 mS cm^{-1} (Table 2). Conductivities are 3.9–6.6 times larger for aqueous solution compared to the fused salt. The low electrolyte conductivity of fused salt leads to high overvoltages compared to the application of the pure aqueous phase. Since both half cell potentials do not follow the increasing trend of cell voltage, there is no increasing kinetic or mass transport inhibition neither in the positive nor the negative half cell (see Fig. 3/a) connected to the observed phenomenon.

In addition to the fact of the formation of a fused salt phase in the porous electrode, it is observed that the effect of the fused salt formation is reversible. During charge, Br_2 is constantly generated at the rate of $+0.037 \text{ mol s}^{-1}$ in the positive half cell caused by galvanostatic charging with a current density of $+50 \text{ mA cm}^{-2}$, which can be calculated from Faraday law. The $[\text{C2Py}]^+(\text{aq})$ cations are present in the solution to a limited extent and their concentration decreases as charging progresses (Fig. 3/c) by formation of fused salt. As a consequence, over the time, less amounts of $[\text{C2Py}]^+$ cations and of fused salt are formed until complete depletion of $[\text{C2Py}]^+(\text{aq})$. In parallel, due to the slow outflow of the fused salt from the positive half cell, the cell voltage decreases, while the clogged pores in the felt electrode are refilled with aqueous electrolyte. The overvoltage in the cell stagnates by peaking and then decreases until it changes into the expected curve of the cell voltage.

3.4. Rise of ohmic resistance during discharge operation

After investigating the anomaly occurring during the charging process, a subsequent task is to investigate the increasing overvoltage during the discharging process, found in Section 3.2. A rise of the ohmic cell resistance shown in Fig. 2/a, marked by “B” can only be attributed to the electrolyte conductivity or the membrane conductivity during discharge as mentioned in Section 3.2 and is investigated further here.

Ionic conductivity of the aqueous electrolyte (Table 2) is not the reason for this ohmic cell resistance: During the discharge process from SoC 100 to 60%, the conductivity increases from 363.4 to 710.2 mS

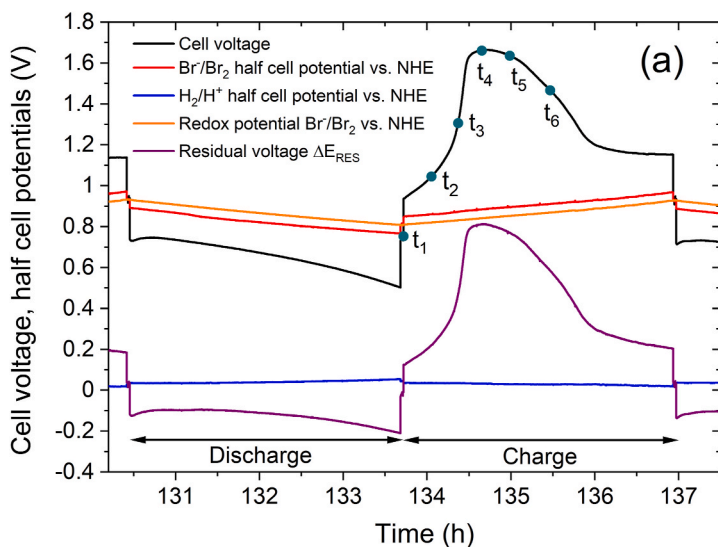
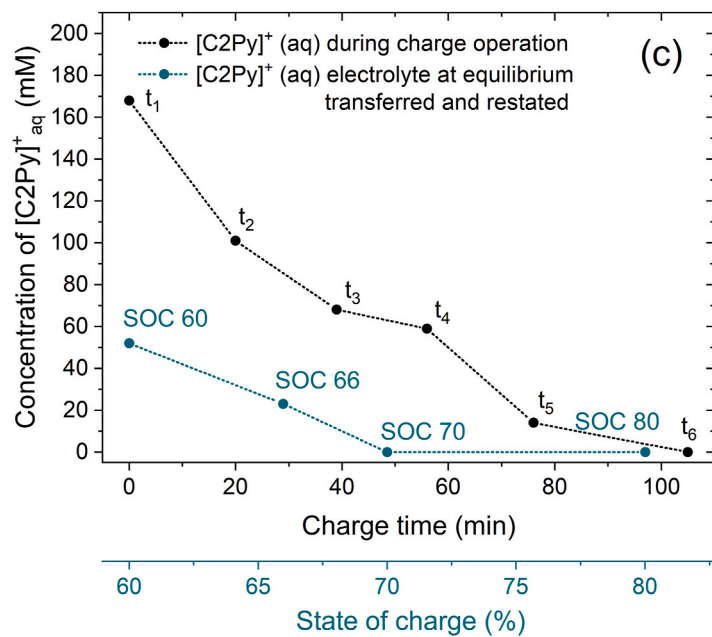
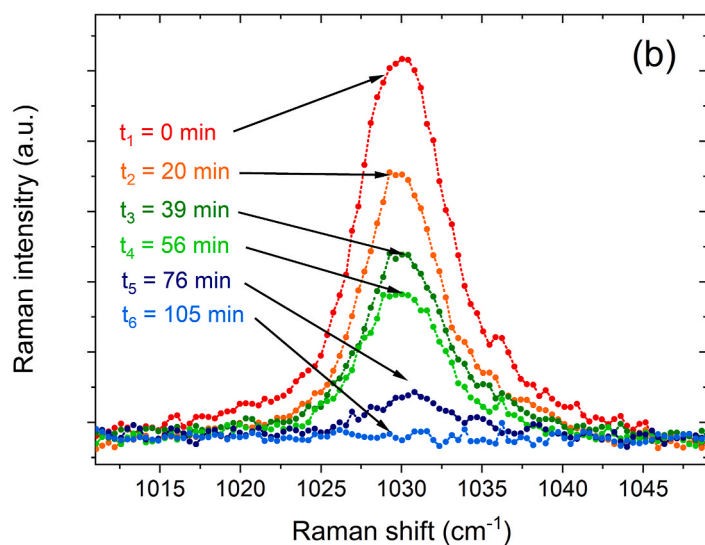


Fig. 3. Investigation of the processes in the bromine half cell during the charge process in (a) occurring voltage peak between SoC 100-60% by sampling of aqueous bulk electrolyte at the times t₁ to t₆. Samples are analysed by (b) Raman spectroscopy for the presence of [C2Py]⁺ cations in aqueous solution at $\tilde{\nu} = 1030.2 \text{ cm}^{-1}$ and (c) plotting the present [C2Py]⁺(aq) concentrations as a function of time t and comparing them with [C2Py]⁺(aq) concentrations at equilibrium on the time scale. [C2Py]⁺(aq) concentrations at equilibrium in (c) are transferred from Table 2 and their position in the diagram is converted to the time scale, as the electrolyte holds a specific SoC for each individual time.



cm^{-1} , as the concentration of conductive protons in the polysulfonate rise [12] during discharge operation.

To investigate this contradiction, the influence of the BCA-containing electrolyte on the membrane functionality is investigated further. The conductivity of perfluorosulfonic acid (PFSA) membranes depends on their saturation with water. 16 water molecules per sulfonate group in the membrane result in a maximum membrane conductivity [59]. To determine the influence of $[\text{C2Py}]^+(\text{aq})$ ions on membrane conductivity, membrane samples are placed in aqueous electrolyte samples with and without $[\text{C2Py}]^+(\text{aq})$ for SoC 0, 33, 60, 70, 80, 90 and 100% ex situ and are examined by FT-IR spectroscopy shown in Fig. 4.

FT-IR measurements show infrared absorption bands of Nafion (Fig. 4) with assigned wavenumbers at $\tilde{\nu} = 1198 \text{ cm}^{-1}$ for symmetric CF_2 stretching [60–62] and $\tilde{\nu} = 1143 \text{ cm}^{-1}$ for asymmetric CF_2 stretching [62–64] of the PTFE backbone in the Nafion 117 membrane. At $\tilde{\nu} = 1302 \text{ cm}^{-1}$ the C–C stretching of the backbone is visible [62]. Characteristic peaks of the side chain are visible at $\tilde{\nu} = 982 \text{ cm}^{-1}$ for the symmetric C–F stretching in $\text{CF}_2\text{-CF-R-CF}_3$ group [62,63,65–67] and at $\tilde{\nu} = 969 \text{ cm}^{-1}$ for C–O–C stretching [62,63,65,67]. A shoulder at $\tilde{\nu} = 1126 \text{ cm}^{-1}$ shows the asymmetric S=O oscillation of the sulfonates [62]. All peaks are known from literature and do not show any FT-IR shift due to treatment with different electrolytes except for the peak at $\tilde{\nu} = 1056 \text{ cm}^{-1}$. The peak with a FT-IR shift of $\tilde{\nu} = 1056\text{--}1060 \text{ cm}^{-1}$ is the symmetrical stretching of the S–O molecular oscillation in the sulfonate group of the side chain in the PFSA [61,66,67].

Depending on the SoC of the electrolyte, rising concentration of $[\text{C2Py}]^+(\text{aq})$ leads to rising interaction with the sulfonate membrane, causing a higher ohmic overvoltage of the membrane: The peak wavenumber at $\tilde{\nu} = 1056\text{--}1060 \text{ cm}^{-1}$ decreases with decreasing SoC, as shown in Fig. 4 with a red arrow. The shift of this S–O oscillation peak is compared in Table 3 to the shift of the peak of the S–O oscillation of a membrane treated in BCA-free $\text{HBr}/\text{Br}_2/\text{H}_2\text{O}$ electrolytes and correlates identically with the increasing concentrations of $[\text{C2Py}]^+(\text{aq})$ in the aqueous electrolyte solution from Table 2.

Table 3 to the shift of the peak of the S–O oscillation of a membrane treated in BCA-free $\text{HBr}/\text{Br}_2/\text{H}_2\text{O}$ electrolytes and correlates identically

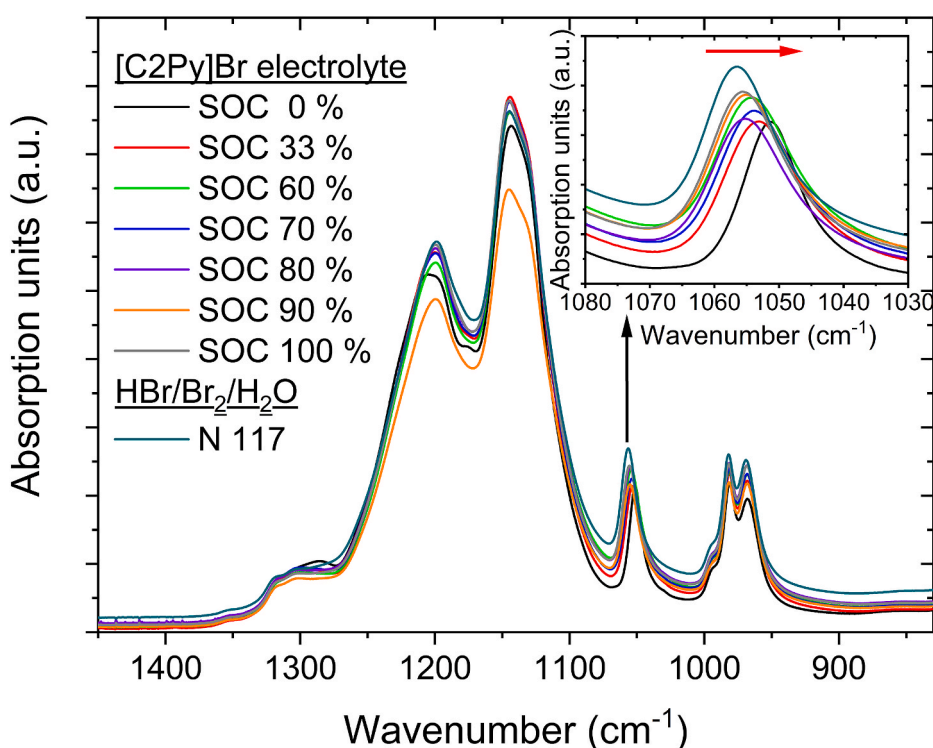


Fig. 4. FT-IR spectra on Nafion 117 membranes with pretreatment in aqueous electrolyte samples with and without $[\text{C2Py}]\text{Br}$ at SoC 100, 90, 80, 70, 60, 33 and 0%. Membrane treated in BCA-free $\text{HBr}/\text{Br}_2/\text{H}_2\text{O}$ without containing $[\text{C2Py}]^+(\text{aq})$ are used as reference membranes. In the embedded diagram the shift of the FT-IR peak for symmetrical stretching oscillation S–O of the sulfonate group is highlighted. The red arrow shows peak shift from N117 without $[\text{C2Py}]^+(\text{aq})$ electrolyte treatment via electrolytes containing $[\text{C2Py}]^+(\text{aq})$ at SOC 100% to SOC 0% with falling wavenumbers. (For interpretation of the references to colour in this figure legend, the reader is referred to the Web version of this article.)

with the increasing concentrations of $[\text{C2Py}]^+(\text{aq})$ in the aqueous electrolyte solution from Table 2. Rising $[\text{C2Py}]^+$ concentrations cause a stronger shift of the S–O peaks downwards to $\tilde{\nu} = 1051.3 \text{ cm}^{-1}$. Hugo et al. [68] describe rising membrane resistances in ex situ investigations of membranes, but without showing quantitative correlation between membrane resistance and actual $[\text{BCA}]^+$ concentration. The interaction of the cation with the sulfonate group is a cation exchange reaction [69]. The organic cation $[\text{C2Py}]^+$ forms with the sulfonate a contact pair, while $[\text{C2Py}]^+$ has a large radius compared to protons and the hydrophobic character of the cation reduces the polarity of the environment. The shift of the S–O peak to lower FT-IR shifts is an effect of the weaker ion pair dipole of the S–O group by the contact pair $\text{SO}_3^-[\text{C2Py}]^+$ [70]. Water is displaced from the membrane by the hydrophobic cation, causing the membrane to dry out [70,71] and limits the transport of protons through the membrane. A higher membrane resistance appears, causing a higher cell overvoltage during discharge operation.

During discharge of the electrolyte $[\text{C2Py}]^+$ is released from the fused salt in higher concentrations than in equilibrated electrolyte samples (Fig. 3/c), which is expected to intensify this effect.

The two effects triggered by the organic BCA cation limiting half-cell and membrane performance have been discussed in detail. Both effects are due to the presence of BCA cations. As a precautionary approach, the performance of the bromine half cell should be improved by avoiding the presence of quaternary ammonium cations. The influence of the investigated electrolytes on the long-term cycle ability of the battery is now to be investigated further.

3.5. Cycle performance and durability over 30 cycles

In previous cell tests, only three cycles have been performed for each cycling SoC range to investigate upcoming phenomena related to the BCA. This results in a temporal snapshot for each SoC range. Based on the results from the previous cell test, this section describes cycling tests of 30 cycles per observation area for SoC 100–80%, SoC 100–70% and SoC 100–60% to investigate long-term performance of the cell and electrolyte. All tests are carried out starting with a discharge process of an electrolyte at SoC 100%.

Table 3FT-IR shift of $\tilde{\nu}_{\text{Peak(S-O)}}$ of FT-IR absorption for Nafion N117.

$\tilde{\nu}_{\text{Peak(S-O)}}$ of $-\text{SO}_3$ group at different N117 samples soaked with different aqueous electrolytes HBr/Br ₂ /H ₂ O including [C2Py]Br							HBr/Br ₂ /H ₂ O pure
SoC 0%	SoC 33%	SoC 60%	SoC 70%	SoC 80%	SoC 90%	SoC 100%	all SoCs
1051.27	1053.20	1054.17	1053.92	1055.13	1055.37	1055.61	1055.61

3.5.1. Voltage characteristics and occurrence of BCA influence

Cell voltages and mass losses of the electrolyte over the number of cycles for tests between SoC 100-80% and 100-60% are measured and shown in Fig. 5. For the purpose of clarity, measurement results for cycling between SoC 100-70% are presented in the ESI (Figure S-2).

For cycling between SoC 100-80%, Fig. 5/a shows a voltage behaviour unaffected by [BCA]⁺ cations, neither in the form of additional peaks during charge, nor an increased ohmic overvoltage during discharge. Cell voltage tends to decrease slightly. A similar performance for the test between SoC 100-70% can be observed shown in the ESI (Figure S-2). For the cycling test between SoC 100-60% (Fig. 5/b) instead, (i) voltage peaks described in Section 3.3, are formed from the 16th cycle during charge operation and (ii) towards the end of the discharge process the cell voltages progressively decrease for all cycles. While for the first 15 cycles only minor influence of [C2Py]⁺ on the cell performance is visible, from cycle 16 onwards [C2Py]⁺ cations in aqueous electrolytes cause performance losses. Effects and dependency on the number of cycles is discussed in the following subchapters.

While cycling between SoC 100-60% has not been possible in the preceding experiment for only three cycles (Section 3.2) due to over-voltages, in the long term test it is feasible during the initial 15 cycles. While during the experiment here in Section 3.5 the fused salt reposes in the glass tank and only the aqueous phase is pumped through the cell, during stepwise cycling in Section 3.2 the mixture of fused salt and aqueous phase has been slightly stirred in the glass tank. By stirring, higher amounts of [C2Py]⁺ are transferred from fused salt to the aqueous phase and lower the cell performance as shown in the experiment in Section 3.3. In addition, the upper cell voltage threshold is enlarged to 3.0 V.

3.5.2. Characteristics of posolyte mass loss by crossover through membrane

In order to maintain the capacity of the battery, the entire amount of electrolyte must be permanently available over the number of cycles. However, crossover can limit the useable capacity. A crossover of the electrolyte across the membrane is measured by the mass change of the posolyte in the tank and is shown in Fig. 5 + ESI Figure S-2 and a strong crossover for all tests is identified. The posolyte mass decreases for all tests sharply over the number of cycles. For cycling between SoC 100-80% posolyte mass loss of approximately 50 g (−33.9 wt%) within 100 h, for SoC 100-70% a loss of 60 g (−40.6 wt%) within 148 h and for SoC 100-60% a mass loss of about 52 g (−35.3 wt%) within 180 h are registered.

A clear, but strongly acidic liquid is collected in a wash bottle at the outlet of the hydrogen half cell for each test. The acidic character is received from HBr. In combination with the mass loss, this indicates a strong crossover of water, HBr and Br₂ from positive to negative half cell during cycling. As Br₂ is reduced with H₂ to HBr at the platinum particles of the hydrogen half cell by catalytic reaction [3], a distinction between passing HBr and Br₂ from mass loss is not feasible.

The sawtooth-shaped trend of the mass change is related to the storage of Br₂ in the fused salt. During charging operation, Br₂ is transferred to the heavy fused salt in the tank and the electrolyte mass in the tank rises, while the mass of the tank is recorded. In parallel the lighter aqueous phase is circulated. For the discharge process, Br₂ enters into the aqueous phase and is stored after reaction as HBr in aqueous phase. The mass in the tank decreases.

3.5.3. Influence of electrolyte crossover on cell voltage for 30 cycles

Crossover of reactants and water influences the cell voltage during operation as well as the open circuit voltage. Average charge and discharge cell voltages of cycling tests are calculated from cell voltages and presented in combination with open circuit voltage in Fig. 6 to focus on durability of cell voltages. Average cell voltages for the SoC 100-80% cycle range slightly decrease for charge from 1.10 V to 1.02 V and for discharge from 0.87 V to 0.78 V. This trend appears more intense during cycling between SoC 100-70% for charge from 1.09 V to 0.95 V and especially during discharge from 0.85 V to 0.66 V. As for tests in the range of SoC 100-60% an influence of [C2Py]⁺ is obvious, cell voltages of this experiment are discussed in Chapter 3.5.4, while here the focus shall be on the effect of crossover of the active species HBr and Br₂ on the cell voltage. Also open cell voltages (Fig. 6/b) show a trend for decreasing cell voltages.

Charge and discharge voltages, open-circuit voltages (Fig. 6) as well as mass of the posolyte decrease with rising number of cycles. All changes indicate a change in electrolyte composition. Due to crossover, in general the amount of Br₂ in relation to the amount of HBr becomes lower in the electrolyte during cycling, leading to lower redox potentials according to Nernst equation and cell voltages over the cycle number for SoC 100-80% and SoC 100-70%. The development of the potentials base on concentration changes of the redox couple [49,72]: If predominantly (i) water from the positive half cell enters the negative half cell, the dissolved bromide and Br₂ in the posolyte get increasingly concentrated. A concentration increase of HBr causes a strong increase in its activity coefficient [72,73] and so its activity. According to Nernst equation, the redox potential of the Br₂/Br[−] and thus the cell voltage both decrease [72]. In parallel (ii) an increased crossover of Br₂ compared to bromide ions from the posolyte through the membrane to the negative half cell leads to the same trend of decreasing cell voltage and open circuit voltage. Both processes (i) and (ii) happen in parallel, are caused by crossover through the membrane and intensify a limited energy output from the battery for rising number of cycles.

3.5.4. Influence of [C2Py]⁺ cations on cell voltages for 30 cycles

For cycling between SoC 100-60% from cycle 16 onwards, increasing cell voltage peaks during the charge process and strongly decreasing voltages towards the end of discharge process are recognized (Fig. 5). The mean charge voltage increases strongly to values > 1.2 V (Fig. 6/a), while over the entire cycle range the mean discharge voltage decreases with a pronounced distance from further experiments (e.g. SoC 100-80%) down to 0.57 V. Anomalies caused by the formation of fused salt in the positive half cell during the charging process and the increasing resistance of the Nafion membrane in contact with [C2Py]⁺(aq) are intensified with number of cycles onwards.

The crossover of Br₂ leads due to the release of [C2Py]⁺ from the fused salt phase in the aqueous phase to a reduced performance in the range SoC 100-60% for both discharge and charge operation. (Concentrations of [C2Py]⁺ have not been measured here.) This tendency is caused by an increasing concentration of [C2Py]Br in the aqueous solution with the number of cycles: Crossover of Br₂ from the positive to the negative half cell causes decreasing Br₂ concentration in the posolyte during cycling. In order to retain the chemical equilibrium of Br₂ between the aqueous phase and the fused salt in the tank, this lack of Br₂ leads to a transfer of Br₂ from the fused salt into the aqueous electrolyte. Following Eq. (2), thereby [C2Py]⁺ is released in the aqueous phase too. During the first 15 cycles this process does not occur or is not visible.

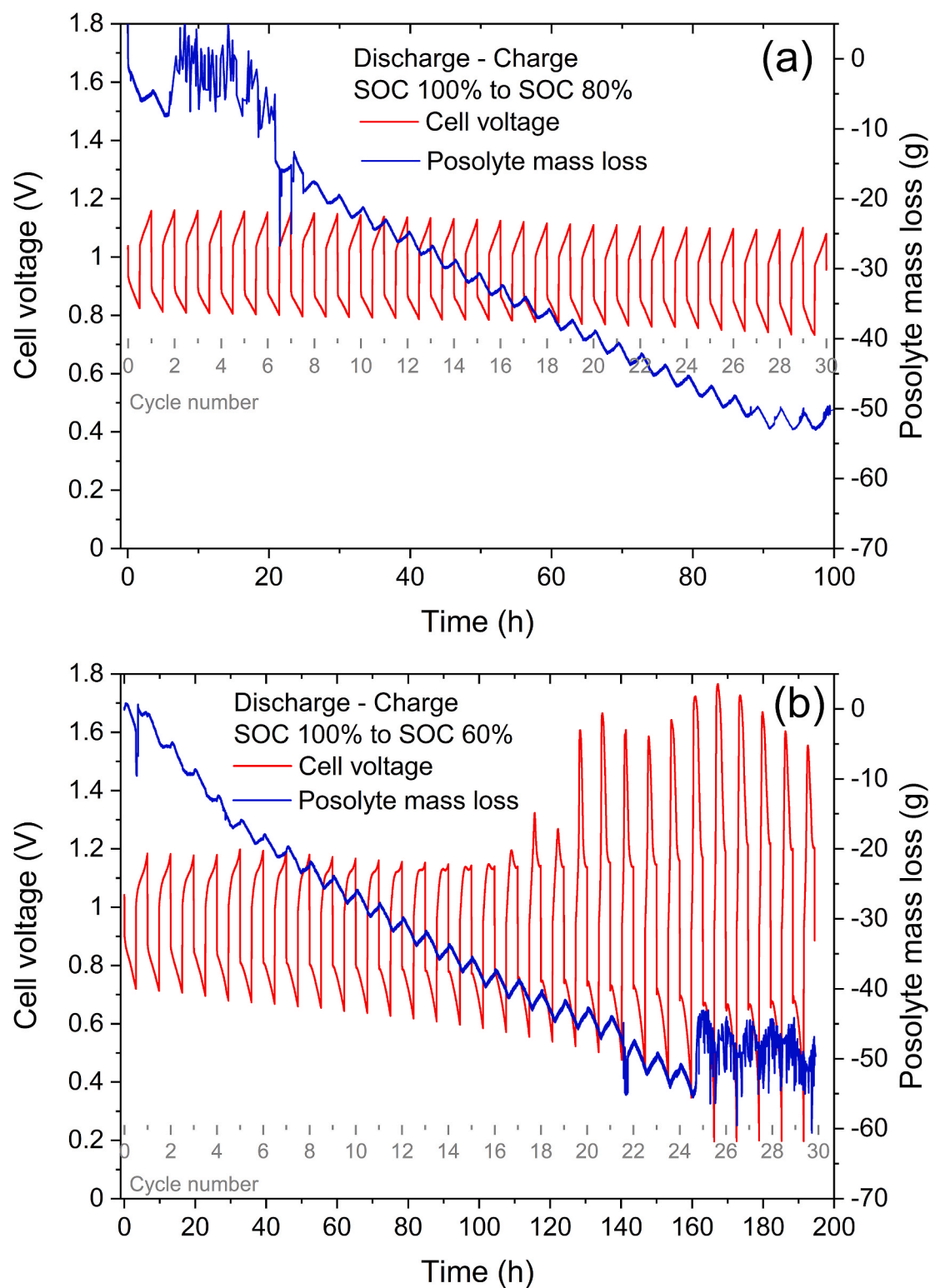


Fig. 5. Cell voltages during the cycling test and mass variations of the bromine electrolyte during galvanostatic cycling tests at $i = \pm 50 \text{ mA cm}^{-2}$ depending on the experiment duration for cycling between (a) SoC 100-80% and (b) SoC 100-60% for 30 cycles each. Numbering in grey colour provides an indication of the number of completed cycles. (For interpretation of the references to colour in this figure legend, the reader is referred to the Web version of this article.)

From cycle 16 on $[\text{C2Py}]^+$ is progressively released into the aqueous phase, pumped into the cell and reduces performance for rising number of cycles.

3.5.5. Durability of membrane performance

To determine membrane performance durability for 30 cycles, ohmic

cell resistances before and after each discharge step are determined by EIS and shown in Fig. 7. All cells filled with posolyte at SoC 100% showed before the first discharge different cell resistances between 1.17 and 1.43 Ohm cm^2 . The ohmic cell resistances before the first discharge depend on the cell setup and are not reproducible for this cell. Regardless of this resistances, clear trends in the ohmic cell resistances

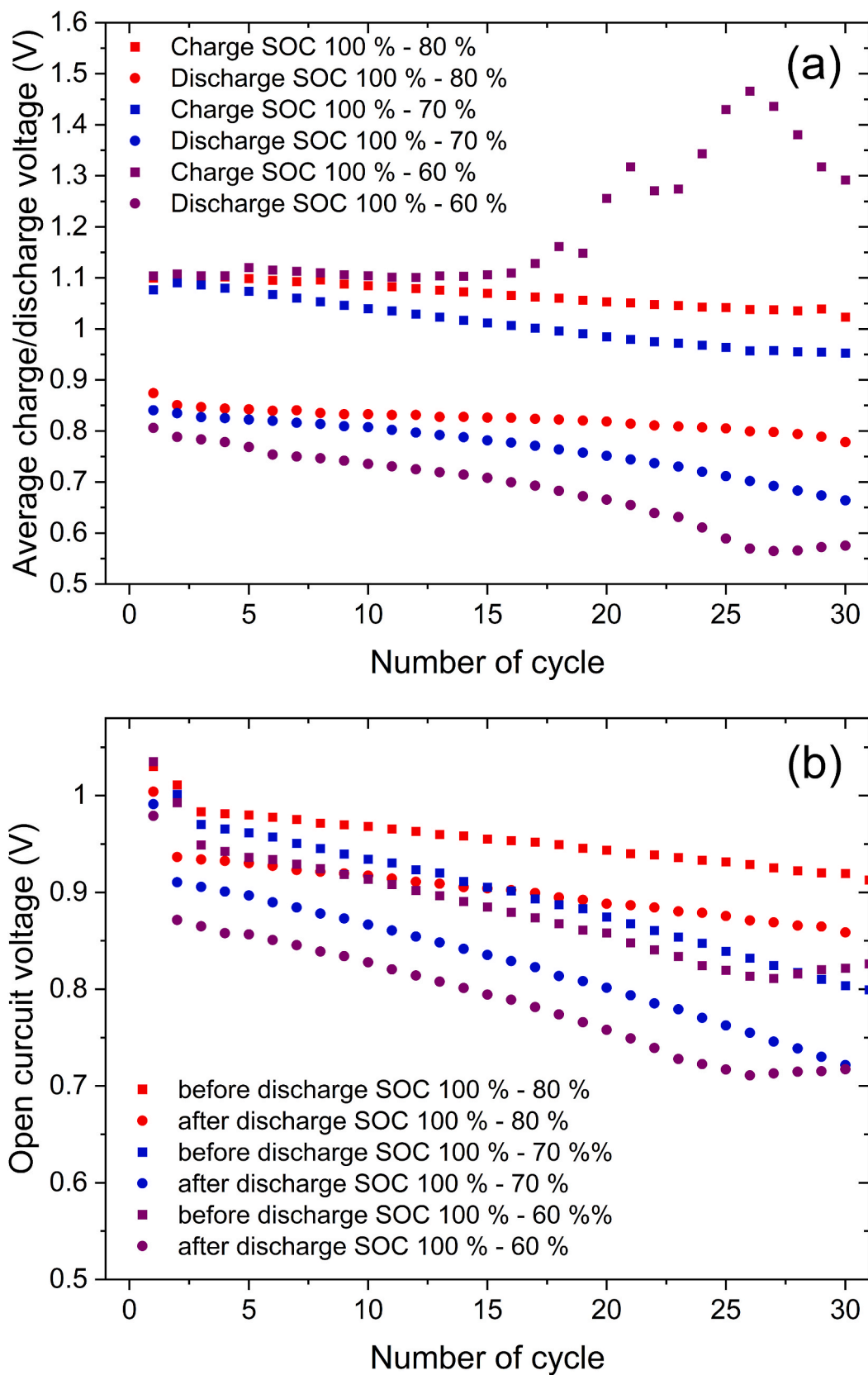


Fig. 6. Cell voltages depending on the operation mode: (a) Average charge (square) and discharge (dot) cell voltages per cycle from the cycle tests for the examined SoC ranges (SoC 100-80% - red, SoC 100-70% - blue, SoC 100-60% - purple) at galvanostatic operation mode with $i = \pm 50 \text{ mA cm}^{-2}$, as well as (b) open circuit voltages before discharge process (square) and after the discharge process (dot) per cycle for the examined SoC ranges (SoC 100-80% - red, SoC 100-70% - blue, SoC 100-60% - purple). (For interpretation of the references to colour in this figure legend, the reader is referred to the Web version of this article.)

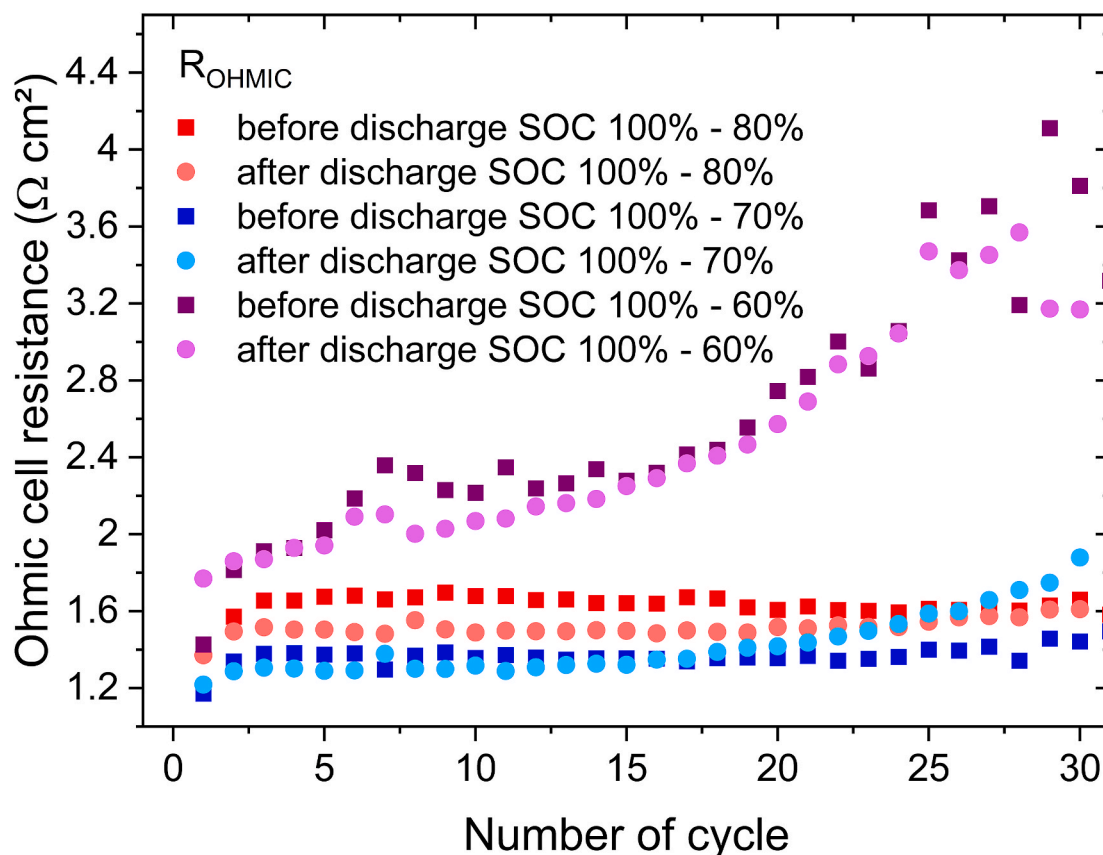


Fig. 7. Ohmic cell resistances before and after the discharge operation based on EIS measurements as a function of the cycle number for galvanostatic cycling between SoC 100-80%, SoC 100-70% and SoC 100-60%. (b) the energy efficiencies (EE) as a function of the cycle number for galvanostatic cycling between SoC 100-80%, SoC 100-70% and SoC 100-60%.

as a function of the number of cycles and depth of discharge are observed and can be separated in two parts, depending of BCA-free aqueous electrolyte phases and BCA-containing aqueous electrolyte phases:

First (i) the ohmic cell resistances are approximately constant in the SoC 100-80% experiment, within a range of 1.48–1.70 $\Omega \text{ cm}^2$ for 30 cycles and for cycling between SoC 100-70% for the first 15 cycles the in the range of 1.29–1.31 $\Omega \text{ cm}^2$. $[\text{C2Py}]^+(\text{aq})$ cations are completely bound in the fused salt and have no effect on the membrane conductivity and on the cell voltages. For both tests a slightly higher resistance before discharge than after discharge operation for each cycle is observed. This differences depend on the conductivity of the aqueous electrolyte with a higher conductivity of 619.4 mS cm^{-2} at SoC 80% than 363.4 mS cm^{-2} at SoC 100%.

For (ii) cycling between SoC 100-70% from cycle 16 onwards, there is an increase in cell resistance after discharge, but a constant lower cell resistance before discharge (Fig. 7). For the cycle experiment SoC 100-60% a continuously increasing ohmic cell resistance after discharging as well as before discharging up to large values of $>3.2 \Omega \text{ cm}^{-2}$ is shown depending on the cycle number. Again, the rising amounts of $[\text{C2Py}]^+(\text{aq})$ released from the fused salt with number of cycles onwards lead to rising membrane resistances. In addition, the increase in membrane resistance for the test between SoC 100-60% is irreversible compared to cycling between SoC 100-70%. Membrane resistance before and after discharge for cycling between SoC 100-60% have similar values within one cycle, even if $[\text{C2Py}]^+$ concentrations in the aqueous posolyte decrease during charge. The interaction between the cation and the membrane is an irreversible process, at least during regular cell cycling.

3.5.6. Cycling efficiencies

Cycling efficiencies are calculated from cell voltage and cell currents for each cycle by application of Eq. S-10 to S-12 (ESI) to evaluate and discuss performance stabilities. A CE of 100% is achieved for all cycles, caused by chosen experimental parameters with limited discharge depth. This CE results in EE and VE having equal values for the respective cycle (Fig. 8). During the last four cycles (27–30) for cycling between SoC 100-60%, discharge operation down to SoC 60% is limited by reaching the cell lower voltage threshold. The SoC of the electrolyte increases from SoC 60%–67% after discharge as depicted in Fig. 8.

If the cell is cycled in the range between SoC 100-80%, EE remains almost constant between 79.5 und 76.0% for 30 cycles (Fig. 8). Here, EE is mainly influenced by the conductivity of cell materials and the aqueous, BCA-free electrolyte. For the cycling between SoC 100-70%, a slight decrease in EE (EE = 69.8% for cycle 30) occurs from the 18th cycle onwards. If the cell is cycled between SoC 100-60%, the EE decreases continuously from EE = 73.5% (cycle 1) to EE = 37.1% (cycle 27). For cycling between SoC 100-70% and SoC 100-60% increasing $[\text{C2Py}]^+$ concentrations in aqueous solution over the number of cycles cause formation of fused salt and low membrane conductivity and lead to a strong decrease of EE.

4. Conclusion

The influence of BCA cations on the performance of the bromine half cell and a cell with a PFSA membrane was investigated using 1-ethylpyridin-1-ium bromide $[\text{C2Py}]\text{Br}$ as an exemplary BCA. Here, $[\text{C2Py}]^+$ cations are present in aqueous solution in the electrolyte and bind Br_2 in form of polybromides in a second fused salt phase. However, $[\text{C2Py}]^+$ cations remain in the aqueous solution and are found to have the

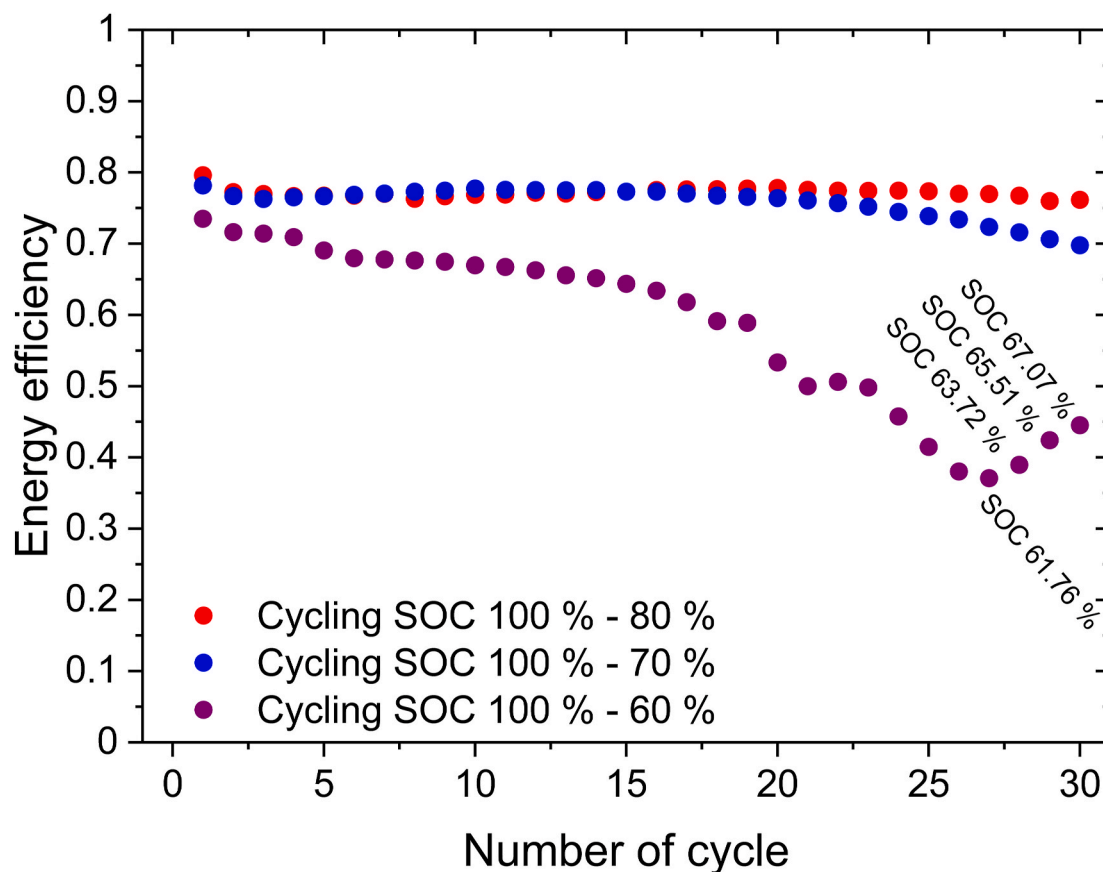


Fig. 8. Energy efficiencies (EE) as a function of the cycle number for galvanostatic cycling between SoC 100-80%, SoC 100-70% and SoC 100-60%.

following adverse effects on the cell performance:

- (1) During charge, Br_2 and $[\text{C2Py}]^+(\text{aq})$ cations are present in the positive half cell and form a fused salt $[\text{C2Py}]\text{Br}_{2n+1}$. Low conductivities of the fused salt in the electrode felt lead to an increase in overvoltage until all cations are bound in the fused salt in the electrode. Therefore, pumping of highly concentrated fused salt through the positive porous electrode is hence not recommended. The phenomenon is reversible and no longer present at the end of the charging process.
- (2) During discharge, $[\text{C2Py}]^+$ cations are released from fused salt phase into the aqueous phase and interact with the sulfonate groups of the PFSA membrane, resulting in a lower membrane conductivity. With rising cycle numbers increasing concentrations of $[\text{C2Py}]^+(\text{aq})$ in the aqueous electrolyte phase lead to increasing membrane resistances. The process is mostly irreversible during cell test.
- (3) Over a longer cycling time, effects of crossover become apparent. In addition to water and HBr , there is increased Br_2 crossover, which leads to lower cell voltages during operation. The depletion of Br_2 in aqueous solution stimulates the release of Br_2 and $[\text{C2Py}]^+$ from the fused salt phase to keep both phases equilibrated. Over the number of cycles, rising $[\text{C2Py}]^+(\text{aq})$ concentrations in the aqueous phase strongly promote the two effects mentioned above in (1) and (2).

$[\text{C2Py}]^+$ dissolved in the aqueous electrolyte results in a reduced usability of the available electrolyte capacity to a maximum 53.9 A h L^{-1} or 30% of the theoretical capacity (179.6 A h L^{-1}). Applying the measured average discharge cell voltage of 0.77 V in this capacity range a useable energy density of 41.5 Wh L^{-1} is achieved from experiments. The performance characteristics are quite limited. Further solutions

must be developed to prevent this problem. First and foremost, the focus here should be on avoiding $[\text{C2Py}]^+$ cations in the aqueous electrolyte solution in the bromine half cell. Compared to vanadium electrolytes, these electrolytes are indeed competitive and a high degree of safety is ensured by the BCA.

Credit author statement

Michael Küttinger: Conceptualization, Methodology, Investigation, Data analysis, Visualisation, Writing – Original Draft, Writing – Editing and Review, Supervision, Resources. Ruben Brunetaud: Methodology, Investigation, Data analysis, Visualisation, Writing – Editing and Review. Jakub K. Włodarczyk: Data analysis, Visualisation, Writing – Editing and Review. Peter Fischer: Writing – Review. Jens Tübke: Funding acquisition.

Declaration of competing interest

The authors declare that they have no known competing financial interests or personal relationships that could have appeared to influence the work reported in this paper.

Acknowledgements

The authors thank the Federal Ministry of Education and Research (BMBF) in the project “PEDUSA” (03XP0135) and the State of Baden-Wuerttemberg/Germany in the project “RedoxWind” for funding. Additionally, the project received funding from the European Union’s Horizon 2020 research programme under the Marie Skłodowska-Curie Grant Agreement no. 765289. The authors acknowledge for funding.

Appendix A. Supplementary data

Supplementary data to this article can be found online at <https://doi.org/10.1016/j.jpowsour.2021.229820>.

References

- [1] T.V. Nguyen, R.F. Savinell, *The Electrochemical Society Interface* (2010) 54–56.
- [2] Y.V. Tolmachev, Russ. J. Electrochem. 50 (2014) 301–316, <https://doi.org/10.1134/S1023193513120069>.
- [3] K.T. Cho, M.C. Tucker, A.Z. Weber, *Energy Technol.* 4 (2016) 655–678, <https://doi.org/10.1002/ente.201500449>.
- [4] K.T. Cho, M.C. Tucker, M. Ding, P. Ridgway, V.S. Battaglia, V. Srinivasan, A. Z. Weber, *ChemPlusChem* 80 (2015) 402–411, <https://doi.org/10.1002/cplu.201402043>.
- [5] K.T. Cho, P. Albertus, V. Battaglia, A. Kojic, V. Srinivasan, A.Z. Weber, *Energy Technol.* 1 (2013) 596–608, <https://doi.org/10.1002/ente.201300108>.
- [6] J. Noack, N. Roznyatovskaya, T. Herr, P. Fischer, *Angew. Chem. Int. Ed.* 54 (2015) 9776–9809, <https://doi.org/10.1002/anie.201410823>.
- [7] F. Beck, P. Rüetschi, *Electrochim. Acta* 45 (2000) 2467–2482, [https://doi.org/10.1016/S0013-4686\(00\)00344-3](https://doi.org/10.1016/S0013-4686(00)00344-3).
- [8] T. Mussini, G. Faita, *Encyclopedia of Electrochemistry of the Elements: Bromine*, Dekker, New York, 1973.
- [9] G.N. Lewis, H. Storch, *J. Am. Chem. Soc.* 39 (1917) 2544–2554, <https://doi.org/10.1021/ja02257a005>.
- [10] M.S. Sherrill, E.F. Izard, *J. Am. Chem. Soc.* 50 (1928) 1665–1675, <https://doi.org/10.1021/ja01393a021>.
- [11] W. Glass, G.H. Boyle, *Fuel Cell Systems: Performance of Hydrogen-Bromine Fuel Cells*, American Chemistry Society, Washington D. C., 1965.
- [12] M. Kittinger, J.K. Włodarczyk, D. Daubner, P. Fischer, J. Tübke, *RSC Adv.* 11 (2021) 5218–5229, <https://doi.org/10.1039/D0RA10721B>.
- [13] R.S. Yeo, D.-T. Chin, *J. Electrochem. Soc.* 127 (1980) 549–555, <https://doi.org/10.1149/1.2129710>.
- [14] M. Schneider, G.P. Rajarathnam, M.E. Easton, A.F. Masters, T. Maschmeyer, A. M. Vassallo, *RSC Adv.* 6 (2016) 110548–110556, <https://doi.org/10.1039/C6RA23446A>.
- [15] R.M.J. Withers, F.P. Lees, *J. Hazard Mater.* 13 (1986) 279–299, [https://doi.org/10.1016/0304-3894\(86\)85002-6](https://doi.org/10.1016/0304-3894(86)85002-6).
- [16] F.P. Worley, *J. Chem. Soc. Trans.* 87 (1905) 1107–1123, <https://doi.org/10.1039/CT9058701107>.
- [17] J.M. Bell, M.L. Buckley, *J. Am. Chem. Soc.* 34 (1912) 14–15, <https://doi.org/10.1021/ja02202a004>.
- [18] W.M. Latimer, *Oxidation Potentials. The Oxidation States of the Elements and Their Potentials in Aqueous Solutions*, Prentice Hall, New York, 1953.
- [19] G. Jones, S. Baeckström, *J. Am. Chem. Soc.* 56 (1934) 1524–1528, <https://doi.org/10.1021/ja01322a022>.
- [20] D.B. Scaife, H.J.V. Tyrrell, *J. Chem. Soc.* (1958) 386–392, https://doi.org/10.1039/JR9580000386_0.
- [21] R.O. Griffith, A. McKeown, A.G. Winn, *Trans. Faraday Soc.* 28 (1932) 101–107, <https://doi.org/10.1039/TF9322800101>.
- [22] M.E. Easton, A.J. Ward, B. Chan, L. Radom, A.F. Masters, T. Maschmeyer, *Phys. Chem. Chem. Phys.* 18 (2016) 7251–7260, <https://doi.org/10.1039/c5cp06913k>.
- [23] J. Fischer, J. Bingle, *J. Am. Chem. Soc.* 77 (1955) 6511–6512, <https://doi.org/10.1021/ja01629a026>.
- [24] S.N. Bajpai, *J. Chem. Eng. Data* 26 (1981) 2–4, <https://doi.org/10.1021/je00023a002>.
- [25] W. Ramsay, S. Young, *J. Chem. Soc. Trans.* 49 (1886) 453–462, <https://doi.org/10.1039/CT8864900453>.
- [26] D. Bryans, B.G. McMillan, M. Spicer, A. Wark, L. Berlouis, *J. Electrochem. Soc.* 164 (2017) A3342–A3348, <https://doi.org/10.1149/2.1651713jes>.
- [27] C. Fabjan, G. Hirss, *Dechema Monographien Band 102* (1985) 149–161.
- [28] K.J. Cathro, K. Cedzynska, D.C. Constable, P.M. Hoobin, *J. Power Sources* 18 (1986) 349–370, [https://doi.org/10.1016/0378-7753\(86\)80091-X](https://doi.org/10.1016/0378-7753(86)80091-X).
- [29] R.A. Putt, M.J. Montgomery, *Metal-Halogen Cell Operation with Storage of Halogen via Organic Complexation External to the Electrochemical Cell*, 1977.
- [30] A.M. Ajami, F.M. Walsh, D.N. Crouse, *Two Phase Electrolytes Used as Halogen Traps in Metal Halogen Secondary Cells and Batteries*, Google Patents, 1976, <http://www.google.com.ar/patents/US4065601>.
- [31] D.J. Eustace, *J. Electrochem. Soc.* 127 (1980) 528–532, <https://doi.org/10.1149/1.2129706>.
- [32] E. Lancry, B.-Z. Magnes, I. Ben-David, M. Freiberg, *ECS Trans* 53 (2013) 107–115, <https://doi.org/10.1149/05307.0107ecst>.
- [33] D. Bryans, L. Berlouis, M. Spicer, B.G. McMillan, A. Wark, *ECS Trans* 77 (2017) 33–36, <https://doi.org/10.1149/07701.0033ecst>.
- [34] G. Poon, A. Parasuraman, T.M. Lim, M. Skyllas-Kazacos, *Electrochim. Acta* 107 (2013) 388–396, <https://doi.org/10.1016/j.electacta.2013.06.084>.
- [35] J.-D. Jeon, H.S. Yang, J. Shim, H.S. Kim, J.H. Yang, *Electrochim. Acta* 127 (2014) 397–402, <https://doi.org/10.1016/j.electacta.2014.02.073>.
- [36] K.J. Cathro, K. Cedzynska, D.C. Constable, *J. Power Sources* 16 (1985) 53–63, [https://doi.org/10.1016/0378-7753\(85\)80003-3](https://doi.org/10.1016/0378-7753(85)80003-3).
- [37] M. Skyllas-Kazacos, G. Kazacos, G. Poon, H. Verseema, *Int. J. Energy Res.* 34 (2010) 182–189, <https://doi.org/10.1002/er.1658>.
- [38] Magnes et al., *Additives for Zinc-Bromine Membraneless Flow Cells*. Bromine Compounds Ltd., 09.05.13.
- [39] W. Kautek, A. Conradi, C. Fabjan, G. Bauer, *Electrochim. Acta* 47 (2001) 815–823, [https://doi.org/10.1016/S0013-4686\(01\)00762-9](https://doi.org/10.1016/S0013-4686(01)00762-9).
- [40] W. Kautek, *J. Electrochem. Soc.* 146 (1999) 3211–3216, <https://doi.org/10.1149/1.1392456>.
- [41] G.P. Rajarathnam, M.E. Easton, M. Schneider, A.F. Masters, T. Maschmeyer, A. M. Vassallo, *RSC Adv.* 6 (2016) 27788–27797, <https://doi.org/10.1039/C6RA03566C>.
- [42] P.M. Hoobin, K.J. Cathro, J.O. Niere, *J. Appl. Electrochem.* 19 (1989) 943–945, <https://doi.org/10.1007/BF01007946>.
- [43] E.S. Sashina, D.A. Kashirskii, G. Janowska, M. Zaborski, *Thermochim. Acta* 568 (2013) 185–188, <https://doi.org/10.1016/j.tca.2013.06.022>.
- [44] A. Aupoix, B. Pégot, G. Vo-Thanh, *Tetrahedron* 66 (2010) 1352–1356, <https://doi.org/10.1016/j.tet.2009.11.110>.
- [45] S.V. Dzhyuba, R.A. Bartsch, *J. Heterocycl. Chem.* 38 (2001) 265–268, <https://doi.org/10.1002/jhet.5570380139>.
- [46] S. Treimer, A. Tang, D.C. Johnson, *Electroanalysis* 14 (2002) 165, [https://doi.org/10.1002/1521-4109\(200202\)14:3<165::AID-ELAN165>3.0.CO;2-6](https://doi.org/10.1002/1521-4109(200202)14:3<165::AID-ELAN165>3.0.CO;2-6).
- [47] W. Vielschich, *Z. für Anal. Chem.* 173 (1960) 84–87, <https://doi.org/10.1007/BF00448719>.
- [48] A. Frumkin, L. Nekrasov, B. Levich, J. Ivanov, *J. Electroanal. Chem.* 1 (1959) 84–90, [https://doi.org/10.1016/0022-0728\(59\)80012-7](https://doi.org/10.1016/0022-0728(59)80012-7), 1959.
- [49] A.J. Bard, L.R. Faulkner, in: *Electrochemical Methods: Fundamentals and Applications*, second ed., John Wiley & Sons, Inc., United States of America, 2001 second ed.
- [50] B. Schrader, W. Meier, *Raman/IR Atlas Organischer Verbindungen/Of Organic Compounds*, Verlag Chemie, Weinheim/Bergstr., 1974.
- [51] M. Fleischmann, P.J. Hendra, A.J. McQuillan, *Chem. Phys. Lett.* 26 (1974) 163–166, [https://doi.org/10.1016/0009-2614\(74\)85388-1](https://doi.org/10.1016/0009-2614(74)85388-1).
- [52] D. Cook, *Can. J. Chem.* 39 (1961) 2009–2024, <https://doi.org/10.1139/v61-271>.
- [53] Christian Blanc, Alfred Rufer, *Understanding the Vanadium Redox Flow Batteries*, in: Jatin Nathwani, Artie Ng (Eds.), *Paths to Sustainable Energy*, December 30th 2010, pp. 333–358, <https://doi.org/10.5772/13338>. Available from: <https://www.intechopen.com/books/paths-to-sustainable-energy/understanding-the-vanadium-redox-flow-batteries>.
- [54] V. Amstutz, K.E. Toghill, C. Comninellis, H.H. Girault, *Bulletin Fachzeitschrift und Verbandsinformationen von Electro Suisse und VSE* 10 (2012) 35–40. <https://www.econbiz.de/Record/les-batteries-redox-pour-le-stockage-d-%C3%A9nergie-amstutz/10010036446>.
- [55] M. Kittinger, J. Noack, R. Elazari, R. Costi, K. Pinkwart, J. Tübke, *International Fuel Battery Forum 2016 - Conference Papers 7* (2016) 46–47.
- [56] X.-Z. Yuan, *Electrochemical Impedance Spectroscopy in PEM Fuel Cells: Fundamentals and Applications*, Springer, London, 2010.
- [57] G. Gershinsky, P. Nanikashvili, R. Elazari, D. Zitoun, *ACS Appl. Energy Mater.* 1 (2018) 4678–4685, <https://doi.org/10.1021/acs.aem.8b00808>.
- [58] K. Saadi, P. Nanikashvili, Z. Tatus-Portnoy, S. Hardisty, V. Shokhen, M. Zysler, D. Zitoun, *J. Power Sources* 422 (2019) 84–91, <https://doi.org/10.1016/j.jpowsour.2019.03.043>.
- [59] K.D. Kreuer, *J. Membr. Sci.* 185 (2001) 29–39, [https://doi.org/10.1016/S0376-7388\(00\)00632-3](https://doi.org/10.1016/S0376-7388(00)00632-3).
- [60] H.W. Starkweather, R.C. Ferguson, D.B. Chase, J.M. Minor, *Macromolecules* 18 (1985) 1684–1686, <https://doi.org/10.1021/ma00151a007>.
- [61] J. Yang, Q. Che, L. Zhou, R. He, R.F. Savinell, *Electrochim. Acta* 56 (2011) 5940–5946, <https://doi.org/10.1016/j.electacta.2011.04.112>.
- [62] E. Moukheiber, *Understanding of the Structure of Perfluorinated Sulfonic Membranes for Fuel Cell*, 2011. PhD thesis, Grenoble.
- [63] Z. Liang, W. Chen, J. Liu, S. Wang, Z. Zhou, W. Li, G. Sun, Q. Xin, *J. Membr. Sci.* 233 (2004) 39–44, <https://doi.org/10.1016/j.memsci.2003.12.008>.
- [64] Y. Wang, Y. Kawano, S.R. Aubuchon, R.A. Palmer, *Macromolecules* 36 (2003) 1138–1146, <https://doi.org/10.1021/ma020156e>.
- [65] M. Laporta, M. Pegoraro, L. Zanderighi, *Phys. Chem. Chem. Phys.* 1 (1999) 4619–4628, <https://doi.org/10.1039/A904460D>.
- [66] J. Ostrowska, A. Narebska, *Colloid Polym. Sci.* 262 (1984) 305–310, <https://doi.org/10.1007/BF01410469>.
- [67] J. Ostrowska, A. Narebska, *Colloid Polym. Sci.* 261 (1983) 93–98, <https://doi.org/10.1007/BF01410686>.
- [68] Y.A. Hugo, N. Mazur, W. Kout, F. Sikkema, Z. Borneman, K. Nijmeijer, *J. Electrochem. Soc.* 166 (2019) A3004–A3010, <https://doi.org/10.1149/2.0951913jes>.
- [69] T. Schäfer, R.E. Di Paolo, R. Franco, J.G. Crespo, *Chemical communications* (Cambridge, England). <https://doi.org/10.1039/B501507C>, 2005, 2594–2596.
- [70] K.M. Cable, K.A. Mauritz, R.B. Moore, *J. Polym. Sci., Part B: Polym. Phys.* 33 (1995) 1065–1072, <https://doi.org/10.1002/polb.1995.090330710>.
- [71] M.N. Szentirmay, N.E. Prieto, C.R. Martin, *J. Phys. Chem.* 89 (1985) 3017–3023, <https://doi.org/10.1021/j100260a013>.
- [72] J. Włodarczyk, M. Kittinger, B. Cantu, P. Fischer, J. Schumacher, in: 16th symposium on modeling and experimental validation of electrochemical energy technologies (ModVal 2019): Book of Abstracts, 2019, p. 93. <https://doi.org/10.21256/ZHAW-2791>.
- [73] W.J. Hamer, Y.-C. Wu, *J. Phys. Chem. Ref. Data* 1 (1972) 1047–1100, <https://doi.org/10.1063/1.3253108>.